Modulation of North American Heat Waves by the Tropical Atlantic Warm Pool

Hosmay Lopez[1], Dongmin Kim[2], Robert West[3], and Ben P. Kirtman[4]

[1]Atlantic Oceanographic and Meteorological Laboratory
[2]CIMAS, University of Miami
[3]Northern Gulf Institute
[4]University of Miami

November 21, 2022

Abstract

Heat waves are among the deadliest natural hazards affecting the United States (US). Therefore, understanding the physical mechanisms modulating their occurrence is essential for improving their predictions and future projections. Using observational data and model simulations, this study finds that the interannual variability of the tropical Atlantic warm pool (AWP, measured as the area enclosed by the 28.5°C sea surface temperature isotherm) modulates heat wave occurrence over the US Great Plains during boreal summer. For example, a larger than normal AWP enhances atmospheric convection over the Caribbean Sea, driving an upper tropospheric anticyclonic anomaly over the Gulf of Mexico and Great Plains, which strengthens subsidence, reduces cloud cover, and increases surface warming. This circulation anomaly thus weakens the Great Plains low-level jet (GPLLJ) and associated moisture transport into the Great Plains, leading to drought conditions and increased heat wave occurrence for most of the US east of the Rockies.

Modulation of North American Heat Waves by the Tropical Atlantic Warm Pool

Hosmay Lopez[1], Dongmin Kim[2], Robert West[3], and Ben Kirtman[2].

[1]Atlantic Oceanographic and Meteorological Laboratory, NOAA, Miami, Florida, USA

[2]Cooperative Institute for Marine and Atmospheric Studies, University of Miami, Miami, Florida, USA

[3]Northern Gulf Institute, Mississippi State University, Mississippi State, MS, USA

Corresponding author address: Hosmay Lopez (NOAA/AOML/PHOD) 4301 Rickenbacker Causeway, Miami, FL 33149, USA. E-mail: Hosmay.Lopez@noaa.gov

Key Points:

- **This work investigates oceanic drivers of interannual variability of North American heat waves**
- **A larger than normal tropical Atlantic warm pool increases the likelihood of heat wave occurrence**
- **The inherently longer predictability of tropical Atlantic SST anomalies could extend predictions of US heat waves**

Abstract

Heat waves are among the deadliest natural hazards affecting the United States (US). Therefore, understanding the physical mechanisms modulating their occurrence is essential for improving their predictions and future projections. Using observational data and model simulations, this study finds that the interannual variability of the tropical Atlantic warm pool (AWP, measured as the area enclosed by the 28.5°C sea surface temperature isotherm) modulates heat wave occurrence over the US Great Plains during boreal summer. For example, a larger than normal AWP enhances atmospheric convection over the Caribbean Sea, driving an upper tropospheric anticyclonic anomaly over the Gulf of Mexico and Great Plains, which strengthens subsidence, reduces cloud cover, and increases surface warming. This circulation anomaly thus weakens the Great Plains low-level jet (GPLLJ) and associated moisture transport into the Great Plains, leading to drought conditions and increased heat wave occurrence for most of the US east of the Rockies.

Plain Language Summary

Extreme heat is responsible for the most weather-related deaths in the US. Using observations and numerical model experiments, this study investigates the potential predictability of heat waves determined by the state of the tropical Atlantic sea surface temperature (SST). During boreal summer (June-July-August; JJA), a larger than normal area of warm SST produces an atmospheric response over the US Great Plains, leading to increased clear-sky conditions, rainfall deficits, surface temperature, and heat wave events. The results of this study suggest a potential seasonal predictability of high-impact extreme heat events, owing to the longer prediction skill of SST.

1. Introduction

The climate community has been interested in the study of North American heat waves for the past several decades, owing to the fact that heat extremes are the number one weather-related cause of death in the United States (US, https://www.weather.gov/hazstat/). These extreme heat events are often linked to large-amplitude atmospheric circulation patterns, such as blocking events (Petoukhov et al. 2013), which operate on weather timescales (i.e., 7-10 days) and are often accompanied by persistent drought and soil moisture deficits (Atlas et al. 2013; Fischer et al. 2007; Donat et al. 2016). Recent advancements in the understanding of these extremes have also led to potential improvement in their predictions. For example, Teng et al. (2013) identified specific teleconnection patterns that modulate US heat waves, which could be forewarned up to 15-20 days in advance. On seasonal timescales, the Pacific North American pattern has been identified as a potential predictor for drought and extreme heat over the western US (Lin et al. 2017; Piao et al. 2016). Sutton and Hodson (2005) identified that Atlantic Ocean sea surface temperature anomalies (SSTA) could influence extreme heat occurrence over North America and Europe. Recently, Lopez et al. (2019) found that enhanced convective activity over the East Asian Monsoon forces a mid-latitude wave train across the Pacific, leading to an enhanced blocking pattern which promotes the occurrence of heat waves in the US Great Plains.

In addition to internal atmospheric processes, land-atmosphere coupling has been shown to modulate heat wave occurrence through soil moisture deficit (Jia et al. 2016; Donat et al. 2016). This is particularly important in the Great Plains, a region where soil moisture and surface air temperature are strongly correlated through longwave radiation, sensible, and latent heating (Koster et al. 2006). A significant amount of the moisture transport and thus precipitation into the Great Plains in boreal spring and summer is through the Great Plains low-level jet (GPLLJ), which is responsible for about one-third of the total moisture transport (Jiang et al. 2007; Cook et al. 2008; Malloy and Kirtman, 2020), where a stronger GPLLJ leads to more precipitation in the Great Plains. Thus, the strength of the GPLLJ is a potential modulator of surface air temperature in the Great Plains.

Several studies have found an increasing trend in summer precipitation over the Great Plains (Kunkel et al. 2013; Janssen et al. 2014), owing to a strengthening of the GPLLJ (Feng et al. 2016). Future projections from CMIP5 models suggest that the GPLLJ strength will increase (Tang et al. 2017), driven by differential heating between land and the adjacent ocean (Cook et al. 2008). Lopez et al. (2018) found a negative correlation between the strength of the GPLLJ and heat wave occurrence over the Great Plains, and argued that in the future, a larger amplitude and enhanced interannual variability of the GPLLJ will add uncertainty in future projections of heat extremes in the Great Plains. That is, an enhanced GPLLJ could alleviate some effects of temperature increase due to anthropogenic climate change by delaying the time of emergence of the anthropogenic signal on top of natural variability.

Interannual variability of the GPLLJ has been linked to tropical Atlantic SSTA variability. Specifically, the Atlantic Warm Pool (AWP, Wang and Enfield 2001), a region encompassing the western tropical Atlantic, Caribbean Sea, and Gulf of Mexico, has been shown to modulate regional precipitation (Wang and Enfield 2001, 2003; Wang et al. 2006, 2008a) as well as tropical cyclone activity (Wang et al. 2006). In addition, Wang and Lee (2007) found that a larger than normal AWP weakens the GPLLJ and associated moisture transport in response to a weakening of the western edge of the North Atlantic Subtropical High, thus modulating moisture transport and precipitation in North America (Algarra et al. 2019; Bishop et al. 2019; Kim et al. 2020). A larger (smaller) than normal AWP is linked to less (more) precipitation in the Great Plains and more (less) Atlantic tropical cyclones (Wang et al. 2006; Wang and Lee 2007; Misra and Li 2014; Liu et al. 2015). A composite analysis based on observed number of heat wave days (see Methods for heat wave definition) over the Great Plains (area averaged from 100°W-85°W and 35°N-45°N) suggests a concurrent warm SST anomaly signal over the Caribbean and tropical Atlantic over the AWP region, as well as a moderately cold SST anomaly over the mid-latitudes in the Pacific Ocean around 40°N (Fig. 1).

Variations of the AWP are predominantly intrinsic to the Atlantic and independent of remote forcing from El Niño-Southern Oscillation (ENSO, Wang et al. 2006; Misra and Chan 2009). While this study focuses on the interannual variability of the AWP, it is worth noting that the AWP has a significant decadal and multidecadal component, owing to its relation to the Atlantic Multidecadal Oscillation (AMO, Enfield et. al. 2001; Wang et al. 2008b). For example, the AWP has been shown to modulate precipitation deficit and heat wave occurrence over northern Mexico and the southwestern US on multidecadal timescales (Ruprich-Robert et al. 2018). However, the interannual variability of heat wave occurrences over the Great Plains in relation to the tropical Atlantic SST has not been investigated. In addition, future projections of surface air temperature show remarkably large uncertainties over the Great Plains relative to other regions, predominantly driven by large natural variability (Supplementary Fig. 1), demonstrating the need to identify natural factors influencing extreme heat events.

This work builds upon the current knowledge of AWP variability and regional atmospheric circulation, tailored towards improving our basic understanding of high impact extreme heatwave events in the US. The remainder of this paper is organized as follows: data and methods are described in section 2, observational links between heat waves and the AWP state are described in section 3, an atmospheric general circulation model (AGCM) experiment prescribing the influence of the AWP is presented in section 4, while conclusion and discussion are presented in section 5.

2. Data and Methods

Observed SSTs are obtained from the Hadley Centre HadSSTv2 product at a 1-degree horizontal resolution for the period of 1900-2019 (Rayner et al. 2003). Atmospheric variables (e.g., vertical profiles of temperature, moisture, geopotential height, wind, and heating rates) are obtained from monthly and daily mean from the Japanese 55-year Reanalysis (JRA55, Kobayashi et al. 2015) for the period of 1955 – present. Extreme temperature and precipitation indices (e.g., highest maximum temperature, drought indices) are obtained from the Hadley Centre (Donat et al. 2013). Daily maximum temperatures are obtained for several meteorological observations over the Great Plains from the NOAA/National Climate for Environmental Information from 1950 - present.

In order to define the AWP index and thus what constitutes large versus small events, we follow the definition of Wang et al. (2006), based on the area-averaged SST exceeding the 28.5°C threshold over the tropical Atlantic basin for each June-July-August (JJA). This area-average is then standardized by the climatological AWP area and then multiplied by 100. This presents the AWP index as a percentage area deviation from the climatological AWP size. As this work is focused on the interannual variations of the AWP, a seven-year running average is removed from the area index to exclude the multidecadal signal of the AWP variability, which is predominantly the AMO component (Supplementary Fig. 2). All analyses are composites of the large and small AWP, determined by the upper and lower terciles of the interannual AWP index respectively (Supplementary Figs. 2 and 3a).

We assess heat waves by the Excess Heat Factor (EHF, Nairm 2009) used in operational forecasts as well as in research studies (Perkins, S. & Alexander 2013). EHF is based on a combination of two excess heat indices as described in (1 and 2):

$$EHI(accl.) = \frac{(T_i + T_{i-1} + T_{i-2})}{3} - \frac{(T_{i-3} + \cdots + T_{i-32})}{30} \quad (1)$$

$$EHI(sig.) = \frac{(T_i + T_{i-1} + T_{i-2})}{3} - T_{95} \quad (2)$$

Here, T_i corresponds to the mean daily surface temperature for day i and T_{95} is the 95th percentile temperature for that given day. *EHI(accl.)* index describes the temperature acclimatization over a 3-day window against the preceding month. *EHI(sig.)* index depicts the anomaly of the same 3-day window against a 95th percentile threshold for that period. This threshold is dependent on the day of the year and geographical location. The *EHF* index is defined by combining equations (1) and (2):

$$EHF = max[1, EHI(accl.)] \times EHI(sig.) \quad (3)$$

Based on (3), a positive *EHF* characterizes heat wave conditions that persist for a minimum of three days.

3. Observed Atlantic Warm Pool and heat waves

The SST changes associated with variations in the AWP size are on the order of 0.5°C relative to climatology (Supplementary Fig. 3e). This SST anomaly, while small, can modulate atmospheric convection and thus circulation given the relatively warm SST mean state (Wang et al., 2006), and is also very similar to the SST anomaly concurrent with heat wave occurrence over the Great Plains (Fig. 1). In addition, the SSTA associated with the large AWP (Supplementary Fig. 3c) is typically larger in magnitude than the small AWP (Supplementary Fig. 3d), evident by the significant skewness in the AWP index (Supplementary Fig. 3a). That is, small AWP are not too distinct from the climatological AWP, whereas the large events consist of mostly an eastward extension of the 28.5°C isotherm away from the Caribbean and Gulf of Mexico. Given the large skewness in the AWP area index, the analysis presented in this work relies on composite averaging rather than regression in order to assess the AWP state (e.g., large versus small) and associated atmospheric circulation.

A composite analysis is performed on several extreme temperature and rainfall indices (Fig. 2) based on the observed state of the AWP. When the AWP is large, the occurrence of warm extremes increases for most of the US Great Plains and is reduced over the Northwestern US. This large-scale pattern is consistent among different extreme temperature indices, e.g., maximum-maximum temperature (Fig. 2b), diurnal temperature range (Fig. 2c), extreme temperature range (Fig. 2d), and number of days above the 90th percentile (Fig. 2e). There is also an associated increase in the number of drought events (Fig. 2f).

To further assess changes in summer extreme heat, we computed the probability density function (PDF) based on the stochastically generated skewed (SGS) distribution of daily maximum temperature during JJA for three stations in the Great Plains (i.e., Chicago, Illinois; St. Louis Missouri; and Oklahoma City, Oklahoma). The SGS distribution measures the non-Gaussian aspect of surface temperature and provides a means to quantify the influence of large versus small AWP on maximum summer temperature, aiding in the assessment of the statistical moments of summer temperature and its PDF. This method was developed to model observed non-Gaussian weather and climate statistics via stochastic noise (Sardeshmukh & Sura 2009) and has been employed to investigate the changes in the statistics of daily wintertime atmospheric circulation (Sardeshmukh et al. 2015) and daily summertime temperature (Lopez et al. 2018). There is a significant shift in the maximum temperature PDF during large AWP periods at all three stations

(Fig. 3), showing an increase in the mean temperature that is statistically significant at the 95th percentile. In addition, summers with larger than normal AWP exhibit enhanced variance (i.e., broadening of the PDF), mostly owing to heavier warm temperature tails. These factors contribute to a decrease in the return period of extreme warm temperature conditions (i.e., extreme temperature days becoming more common) during large AWP summers.

A composite difference of large minus small AWP summers of JJA area-averaged (100°W-85°W and 35°N-45°N) vertical profiles of temperature and geopotential height show a classic "heat-dome" warm anomaly and positive geopotential height anomaly throughout the column up to 150 hPa (Supplementary Fig. 4). Analysis of different estimated heating rates from JRA55 shows that adiabatic heating (i.e., subsidence) dominates up to 200 hPa, with significant longwave cooling rates and diffusive heating rates at low levels, likely associated with clear sky and significant surface warming. Overall, the total heating rate profile indicates a net warming (cooling) above (below) 700 hPa, with a maximum heating rate anomaly around 350 hPa, which explains the observed "heat-dome" structure in the temperature and geopotential height profiles.

To assess circulation changes associated with the state of the AWP, a composite analysis is performed during large minus small AWP summers for the barotropic (Fig. 4a; 850hPa + 200hPa) and baroclinic (Fig. 4b; 850hPa - 200hPa) streamfunction responses to the AWP index. Note that there is strong ridging over the eastern half of the US associated with a barotropic anticyclonic response to the large AWP (Fig. 4a), which also produces a baroclinic Gill-type atmospheric response (Gill 1980) over the Gulf of Mexico (Fig. 4b). This is accompanied by a zonal dipole in the 200 hPa velocity potential (Supplementary Fig. 5b), with upper-level divergence (convergence) over the tropical Atlantic (Pacific) and associated rising (sinking) motion centered at 15°N (Supplementary Fig. 5d). The ridge over the Great Plains is part of a larger anticyclonic anomaly, which extends from the Northern Caribbean and Gulf of Mexico (Supplementary Fig. 5a). This anticyclonic anomaly serves as an "omega block" pattern with cyclonic anomalies upstream and downstream, blocking the climatological westerly flow from 30°N-50°N over the Great Plains and eastern US. Analysis of the Rossby wave source finds both tropical and extratropical origins for the anomalous circulation (Supplementary Fig. 5c). The tropical Rossby wave source shows a dipole structure with cyclonic (anticyclonic) sources over the equator in the Atlantic (Pacific) basin, primarily driven by planetary vorticity advection associated with the divergent wind anomaly. In contrast, the mid-latitude features an anticyclonic (cyclonic) Rossby wave source over the Gulf of Mexico and eastern US (eastern extratropical Pacific), which explains the "omega-like" streamfunction response around 40°N.

The circulation anomaly extracted from compositing the AWP size is consistent with the observed increase in heat wave occurrence over the Great Plains during large AWP summers (Fig. 2). However, it remains unclear whether this anomalous pattern is a significant feature of the regional boreal summer circulation. As such, we perform an empirical orthogonal function (EOF) analysis of the 200 hPa streamfunction anomalies over JJA. The principal component (i.e., timeseries) is then regressed onto relevant circulation anomalies and Rossby wave sources. It is noted that the second most dominant EOF mode (Supplementary Fig. 6), which explains ~10% of the total variance of JJA 200 hPa streamfunction anomalies, resembles the anomalous circulation and Rossby wave sources associated with the AWP size (Supplementary Fig. 5). In addition, this second EOF mode is related to a tropical Atlantic warm SST anomaly (Supplementary Fig. 7) similar to the SST anomalies concurrent with heat wave occurrence (Fig. 1) and those associated with large AWP (Supplementary Fig. 3e). That is, the correlated circulation anomalies associated with the AWP state are a dominant mode of interannual JJA variability and responsible for heat wave modulation. Nonetheless, it remains to be shown whether the AWP is actively driving this atmospheric response, which is discussed next.

In addition to circulation changes, the composite of large minus small AWP shows reduced precipitation, enhanced moisture transport divergence, and a negative standard precipitation index (Supplementary Fig. 8) indicative of drought conditions. To further assess the origin of the drought conditions, a cross section analysis along 30°S from 110°W to 85°W is performed to depict the main core region of the GPLLJ. Supplementary Fig. 8d shows the JJA climatological meridional moisture transport $(vq)_{climo}$ (black contour) and large minus small AWP $(vq)_{Large\ AWP} - (vq)_{Small\ AWP}$ (color), where v is the meridional wind and q depicts specific humidity. There is a reduction in the moisture transport during summers where the AWP is large. Further analysis shows that changes in the circulation (e.g., changes in the meridional low-level flow, Supplementary Fig. 8e) rather than changes in moisture (e.g., changes in specific humidity, Supplementary Fig. 8f) are responsible for the reduction in GPLLJ-related moisture transport associated with AWP area index variability.

4. AGCM experiment

The changes in atmospheric circulation presented earlier could be influenced by factors external to the AWP. For example, the GPLLJ has been shown to be influenced by tropical Pacific SSTAs (Weaver et al. 2009; Krishnamurthy et al. 2015). In addition, decadal variability of US drought occurrence could also be influenced remotely by Pacific SSTAs (Mo et al. 2009). Kim et al. (2020) showed that the interbasin SST contrast between the tropical Pacific and Atlantic modulates the GPLLJ and thus late summer and early fall US precipitation, while Zhang et al. (2021) showed that Gulf Stream - North Atlantic Subtropical High (NASH) interactions affect southeast US rainfall and moisture transport from the Gulf of Mexico. Therefore, in order to isolate the effect of the interannual AWP area index, we perform several atmospheric general circulation model (AGCM) experiments. We prescribe SSTA to the Community Atmosphere Model version 6 (CAM6) coupled to the Community Land Model version 5 (CLM5), which are both part of the Community Earth System Model version 2 (CESM2). First, the control case is integrated by prescribing the SST climatology globally based on the 1979-2018 observing period. Then, a model experiment is conducted where SST is prescribed based on cyclical 1979-2018 SST only over the tropical Atlantic and North Pacific and is held to climatology elsewhere (Supplementary Fig. 9). Variations in North Pacific SSTs are included in the AGCM run because it is a recurrent feature associated with AWP variability (Fig.1 and Supplementary Fig. 7) and thus could be key in setting up the large-scale atmospheric pattern associated with heatwaves. Both model experiments are integrated for 200 years under a year-2000 anthropogenic atmosphere composition (i.e., CESM2 component set F2000; https://www.cesm.ucar.edu/models/cesm2/config/compsets.html). Note that the AGCM is able to accurately simulate the observed 95th percentile threshold of 2-meter air temperature, which is the temperature threshold used here in defining heat waves (Supplementary Fig. 10), as well as the mean JJA upper-level circulation (Supplementary Fig. 11).

Analysis of these AGCM experiments is presented here in terms of the differences between large and small AWP years. Note that similar to observations, the AGCM model experiment depicts a barotropic anticyclonic circulation anomaly and a blocked flow pattern over central North America when the AWP is large (Fig. 4c) and a Gill-response over the Gulf of Mexico (Fig. 4d). The upper-level divergent flow and the Rossby wave sources are consistent with the observed composite analysis (Fig. 4a and b). However, the AGCM response to SST forcing appears to have a slight north and west shift in the 200 hPa streamfunction response (Supplementary Fig. 12) when compared to observations (Supplementary Fig. 5), which may be caused by a slight northward bias in the mean JJA zonal and meridional wind as well as an easterly bias in the tropics (Supplementary Fig. 11). Nevertheless, it is evident that the AWP is indeed a modulator of a major mode of interannual variability responsible for heat wave occurrence over the US.

To quantify the impact on the number of heat wave days, we followed equations 1-3, where the daily T_{95} percentile temperature is computed from the 200-year control simulation. Then, an excess heat factor is computed for the AGCM model experiments relative to the T_{95} from the control simulation. Supplementary Figure 13 shows the relative change in the number of heat wave days during JJA, computed by the difference in heat wave days between the large minus small AWP composite and normalized by the total heat wave days. Note that there is a ~40% increase in the heat wave days over most of the Great Plains and Southeastern US for boreal summers where the AWP is larger than normal. This is consistent with the observed results, validating the hypothesis that a large AWP leads to more extreme heat in the US Great Plains during boreal summer.

5. Discussion

Enhancing our understanding of the physical mechanisms controlling the occurrence of high impact extreme events such as heat waves is important, not only for improving their predictions but for understanding their future projections. This work identifies the interannual variability of the AWP as a natural modulator of heat wave occurrence over the US Great Plains, aided by the use of observational records and atmospheric model experiments from a state-of-the-art general circulation model. Based on an area index, we show that when the AWP is larger than normal, enhanced atmospheric convection over the Caribbean Sea produces an upper troposphere zonal divergence pattern with divergence (convergence) over the Atlantic (Pacific) basin centered around 15°N and a Gill-type atmospheric response (Gill 1980) over the Gulf of Mexico (Fig. 4).

This in turn modulates Rossby wave sources that produce an anticyclonic blocking pattern over the Great Plains, which enhances subsidence, clear skies and significant surface warming, leading to a heat dome. In addition, a large AWP weakens the GPLLJ and associated moisture transport into the Great Plains, eventually leading to drought conditions and increased heat wave occurrence for most of the US east of the Rockies. As the Great Plains is a region of strong coupling between surface air temperature and soil moisture where soil moisture is a limiting constraint on latent heating (Koster et al., 2006; Seneviratne et al. 2010), reduced precipitation increases the likelihood of extreme temperature and heat wave days.

These results present a useful mechanism identifying natural drivers of heat wave occurrence over the Great Plains on interannual timescales. While the internal atmospheric dynamics involving heat waves (e.g., Rossby wave breaking, blocking events) and coupled land-atmospheric processes (e.g., soil moisture-air temperature coupling) operate on relatively fast timescales from days to a few weeks, tropical Atlantic SSTA associated with the AWP have been shown to possess skillful predictions on seasonal timescales (3-4 months, Misra and Li 2014). Therefore, the inherently longer predictability of tropical Atlantic SSTA could serve as an opportunity to extend the predictions of US heat waves beyond the synoptic and sub-seasonal timescales. In addition, since future projections of heat waves are more uncertain for the Great Plains (Lopez et al. 2018) due to the large natural variability in surface temperature (Supplementary Fig. 1), identifying natural factors (e.g., AWP size) modulating these extremes will aid in not only their prediction but better understanding of their future projections.

Acknowledgement

This research was carried out in part under the auspices of the Cooperative Institute for Marine and Atmospheric Studies, a cooperative institute of the University of Miami and the National Oceanic and Atmospheric Administration (NOAA), cooperative agreement NA 20OAR4320472. Hosmay Lopez acknowledges support from NOAA/CPO/MAPP Award NA19OAR4310282.

Open Research

Hadley Centre HadSSTv2 product for the period of 1900-2019 was obtained from https://www.metoffice.gov.uk/hadobs/hadisst/ (Rayner et al. 2003). The Japanese 55-year Reanalysis was obtained from https://rda.ucar.edu/datasets/ds628.0/ (JRA55, Kobayashi et al. 2015) for the period of 1955 – present. Extreme temperature and precipitation indices were provided by the Met Office Hadley Centre https://www.metoffice.gov.uk/hadobs/hadex2/ (Donat et al. 2013). Daily maximum temperatures are obtained for several meteorological observations over the Great Plains from the NOAA/National Climate for Environmental Information from 1950 – present https://www.ncdc.noaa.gov/cdo-web/search?datasetid=GHCND. Details on installing and running the CESM2 can be found at https://github.com/ESCOMP/CESM.

References

Algarra, I., Eiras-Barca, J., Miguez-Macho, G., Nieto, R., & Gimeno, L. (2019). On the assessment of the moisture transport by the Great Plains low-level jet. Earth System Dynamics, 2019(10), 107–119. https://doi.org/10.5194/esd-10-107-2019

Atlas, R., Wolfson, N., & Terry, J. (1993). The effect of SST and soil moisture anomalies on GLA model simulations of the 1988 U.S. summer drought. Journal of Climate, 6(11), 2034–2048. https://doi.org/10.1175/1520-0442(1993)0062.0.CO;2

Bishop, D. A., Williams, A. P., Seager, R., Fiore, A. M., Cook, B. I., Mankin, J. S., et al. (2019). Investigating the causes of increased twentieth-century fall precipitation over the southeastern United States. Journal of Climate, 32(2), 575–590. https://doi.org/10.1175/ JCLI-D-18-0244.1

Cook, K. H., Vizy, E. K., Launer, Z. S., & Patricola, C. M. (2008). Springtime intensification of the Great Plains low-level jet and Midwest precipitation in GCM simulations of the twenty-first century. *Journal of Climate*, *21*(23), 6321-6340.

Donat, M. G., Alexander, L. V., Yang, H., Durre, I., Vose, R., Dunn, R. J. H., ... & Kitching, S. (2013). Updated analyses of temperature and precipitation extreme indices since the beginning of the twentieth century: The HadEX2 dataset. *Journal of Geophysical Research: Atmospheres*, *118*(5), 2098-2118.

Donat, M. G., A. D. King, J. T. Overpeck, L. V. Alexander, I. Durre, and D. J. Karoly, 2016: Extraordinary heat during the 1930s US Dust Bowl and associated large-scale conditions. Climate Dyn., 46, 413–426, https://doi.org/10.1007/s00382-015-2590-5.

Enfield, D. B., Mestas-Nuñez, A. M., & Trimble, P. J. (2001). The Atlantic multidecadal oscillation and its relation to rainfall and river flows in the continental US. *Geophysical Research Letters*, *28*(10), 2077-2080.

Feng, Z., Leung, L. R., Hagos, S., Houze, R. A., Burleyson, C. D., & Balaguru, K. (2016). More frequent intense and long-lived storms dominate the springtime trend in central US rainfall. *Nature communications*, *7*(1), 1-8.

Fischer, E. M., Seneviratne, S. I., Vidale, P. L., Lüthi, D., & Schär, C. (2007). Soil moisture–atmosphere interactions during the 2003 European summer heat wave. *Journal of Climate*, *20*(20), 5081-5099.

Gill, A. E. (1980). Some simple solutions for heat-induced tropical circulation. Quarterly Journal of the Royal Meteorological Society, 106(449), 447–462. https://doi.org/10.1002/qj.49710644905

Janssen, E., Wuebbles, D. J., Kunkel, K. E., Olsen, S. C., & Goodman, A. (2014). Observational- and model-based trends and projections of extreme precipitation over the contiguous United States. *Earth's Future*, *2*(2), 99-113.

Jia, L., and Coauthors, 2016: The roles of radiative forcing, sea surface temperatures, and atmospheric and land initial conditions in U.S. summer warming episodes. J. Climate, 29, 4121–4135, https://doi.org/10.1175/JCLI-D-15-0471.1.

Jiang, X., Lau, N. C., Held, I. M., & Ploshay, J. J. (2007). Mechanisms of the Great Plains low-level jet as simulated in an AGCM. *Journal of the Atmospheric Sciences*, *64*(2), 532-547.

Kobayashi, S., et al. (2015), The JRA-55 reanalysis: General specifications and basic characteristics, J. Meteorol. Soc. Jpn., 93, 5–48, doi:10.2151/ jmsj.2015-001.

Kim, D., Lee, S. K., Lopez, H., Foltz, G. R., Misra, V., & Kumar, A. (2020). On the role of Pacific-Atlantic SST contrast and associated Caribbean Sea convection in August–October US regional rainfall variability. *Geophysical Research Letters*, *47*(11), e2020GL087736.

Koster, R. D., Guo, Z. C., Dirmeyer, P. A., Bonan, G., Chan, E., Cox, P., et al. (2006). GLACE: The Global Land–Atmosphere Coupling Experiment. Part I: Overview. Journal of Hydrometeorology, 7, 590–610

Krishnamurthy, L., Vecchi, G. A., Msadek, R., Wittenberg, A., Delworth, T. L., & Zeng, F. (2015). The seasonality of the Great Plains low-level jet and ENSO relationship. *Journal of Climate*, *28*(11), 4525-4544.

Kunkel, K. E., Karl, T. R., Brooks, H., Kossin, J., Lawrimore, J. H., Arndt, D., ... & Wuebbles, D. (2013). Monitoring and understanding trends in extreme storms: State of knowledge. *Bulletin of the American Meteorological Society*, *94*(4), 499-514.

Lin, Y. H., Hipps, L. E., Wang, S. Y. S., & Yoon, J. H. (2017). Empirical and modeling analyses of the circulation influences on California precipitation deficits. Atmospheric Science Letters, 18(1), 19–28. https://doi.org/10.1002/asl.719

Liu, H., Wang, C., Lee, S. K., & Enfield, D. (2015). Inhomogeneous influence of the Atlantic warm pool on United States precipitation. *Atmospheric Science Letters*, *16*(1), 63-69.

Lopez, H., West, R., Dong, S., Goni, G., Kirtman, B., Lee, S. K., & Atlas, R. (2018). Early emergence of anthropogenically forced heat waves in the western United States and Great Lakes. *Nature Climate Change*, *8*(5), 414-420.

Lopez, H., Lee, S. K., Dong, S., Goni, G., Kirtman, B., Atlas, R., & Kumar, A. (2019). East Asian monsoon as a modulator of US Great Plains heat waves. *Journal of Geophysical Research: Atmospheres*, *124*(12), 6342-6358.

Malloy, K. M., & Kirtman, B. P. (2020). Predictability of midsummer Great Plains low-level jet and associated precipitation. *Weather and Forecasting*, *35*(1), 215-235.

Misra, V., S. Chan, R. Wu, and E. Chassignet (2009), Air-sea interaction over the Atlantic Warm Pool, Geophys. Res. Lett., 36, L15702, doi:10.1029/2009GL038737.

Misra, V., & Li, H. (2014). The seasonal climate predictability of the Atlantic Warm Pool and its teleconnections. *Geophysical Research Letters*, *41*(2), 661-666.

Mo, K. C., Schemm, J. K. E., & Yoo, S. H. (2009). Influence of ENSO and the Atlantic multidecadal oscillation on drought over the United States. *Journal of Climate*, *22*(22), 5962-5982.

Nairn, J. Fawcett, R. & Ray, R. Defining and predicting Excessive Heat events, a National system, paper presented at Proceedings of the CAWCR modelling workshop: understanding high impact weather, Citeseer (2009).

Perkins, S. & Alexander, L. On the measurement of heat waves, *Journal of Climate*, **26**(13), 4500-4517 (2013).

Petoukhov, V., Rahmstorf, S., Petri, S., & Schellnhuber, H. J. (2013). Quasiresonant amplification of planetary waves and recent Northern Hemisphere weather extremes. Proceedings of the National Academy of Sciences of the United States of America, 110(14), 5336–5341. https://doi.org/10.1073/pnas.1222000110

Piao, L., Fu, Z., & Yuan, N. (2016). "Intrinsic" correlations and their temporal evolutions between winter-time PNA/EPW and winter drought in the west United States. Scientific Reports, 6(1), 19958. https://doi.org/10.1038/srep19958

Rayner, N. A. A., Parker, D. E., Horton, E. B., Folland, C. K., Alexander, L. V., Rowell, D. P., ... & Kaplan, A. (2003). Global analyses of sea surface temperature, sea ice, and night marine air temperature since the late nineteenth century. *Journal of Geophysical Research: Atmospheres*, *108*(D14).

Ruprich-Robert, Y., Delworth, T., Msadek, R., Castruccio, F., Yeager, S., & Danabasoglu, G. (2018). Impacts of the Atlantic multidecadal variability on North American summer climate and heat waves. *Journal of Climate*, *31*(9), 3679-3700.

Sardeshmukh, P. D., & Sura, P. (2009). Reconciling non-Gaussian climate statistics with linear dynamics. *Journal of Climate*, *22*(5), 1193-1207.

Sardeshmukh, P. D., Compo, G. P., & Penland, C. (2015). Need for caution in interpreting extreme weather statistics. *Journal of Climate*, *28*(23), 9166-9187.

Seneviratne, S. I., Corti, T., Davin, E. L., Hirschi, M., Jaeger, E. B., Lehner, I., et al. (2010). Investigating soil moisture–climate interactions in a changing climate: A review. Earth-Science Reviews, 99(3-4), 125–161. https://doi.org/10.1016/j.earscirev.2010.02.004

Sutton, R. T., & Hodson, D. L. (2005). Atlantic Ocean forcing of North American and European summer climate. Science, 309(5731), 115–118

Tang, Y., Winkler, J., Zhong, S., Bian, X., Doubler, D., Yu, L., & Walters, C. (2017). Future changes in the climatology of the Great Plains low-level jet derived from fine resolution multi-model simulations. *Scientific reports*, *7*(1), 1-10.

Teng, H., Branstator, G., Wang, H., Meehl, G. A., & Washington, W. M. (2013). Probability of US heat waves affected by a subseasonal planetary wave pattern. Nature Geoscience, 6(12), 1056

Wang, C., and D. B. Enfield (2001), The tropical Western Hemisphere Warm Pool, Geophys. Res. Lett., 28, 1635 – 1638, doi:10.1029/ 2000GL011763.

Wang, C., and D. B. Enfield (2003), A further study of the tropical Western Hemisphere Warm Pool, J. Clim., 6, 1476 – 1493.

Wang, C., D. B. Enfield, S.-K. Lee, and C. W. Landsea (2006), Influences of the Atlantic Warm Pool on Western Hemisphere summer rainfall and Atlantic hurricanes, J. Clim., 19, 3011 – 3028, doi:10.1175/JCLI3770.1.

Wang, C., & Lee, S. K. (2007). Atlantic warm pool, Caribbean low-level jet, and their potential impact on Atlantic hurricanes. *Geophysical research letters*, *34*(2).

Wang, C., S.-K. Lee, and D. B. Enfield (2008a), Climate response to anomalously large and small Atlantic warm pools during the summer, J. Clim., 21, 2437 – 2450, doi:10.1175/2007JCLI2029.1.

Wang, C., S.-K. Lee, and D. B. Enfield (2008b), Atlantic Warm Pool acting as a link between Atlantic Multidecadal Oscillation and Atlantic tropical cyclone activity, Geochem. Geophys. Geosyst., 9, Q05V03, doi:10.1029/ 2007GC001809.

Weaver, S. J., Schubert, S., & Wang, H. (2009). Warm season variations in the low-level circulation and precipitation over the central United States in observations, AMIP simulations, and idealized SST experiments. *Journal of Climate*, *22*(20), 5401-5420.

Zhang, W., Kirtman, B. P., Siqueira, L., Xiang, B., Infanti, J. M., & Perlin, N. (2021). The Influence of a Resolved Gulf Stream on the Decadal Variability of Southeast US Rainfall. https://doi.org/10.1002/essoar.10507067.1

Figure captions

Figure 1. Composite difference of heat wave day percentage changes (%, contour over land) and SST anomalies (°C, shading over oceans) based on heat wave occurrence over the Great Plains. The composite is presented in terms of the difference between the upper and lower terciles of the number of heat wave days averaged from 100°W-85°W and 35°N-45°N.

Figure 2. Composite difference of large minus small Atlantic Warm Pool years during JJA for: a) number of heat wave days, b) highest maximum temperature, c) diurnal temperature range, d) extreme temperature range, e) number of days with maximum temperature exceeding the 90th percentile, and f) number of drought days. Panels a, e, and f have units of percentage as defined by the number of events during large minus small AWP divided by the total events and multiplied by 100 such that a 100% increase translates into a doubling of the events.

Figure 3. Probability density function (PDF) of daily maximum temperature during JJA for large (red) and small (blue) AWP years for three stations in the Great Plains and Midwest; a) Chicago

O'Hare International Airport, Illinois, b) St. Louis, Missouri, and c) Oklahoma City, Oklahoma. The mean maximum temperature (μ) and confidence interval at 95% level based on a student-T test, standard deviation (σ), and return period (days) of the 95th percentile temperature is also shown.

Figure 4. Composite difference of large minus small AWP years during JJA for observed a) barotropic streamfunction response (850hPa + 200hPa, $10^6\ s^{-1}$) and b) baroclinic streamfunction response (850hPa - 200hPa, $10^6\ s^{-1}$). Vectors depict the rotational wind component associated with the streamfunction composites. Panels c) and d) are similar to a) and b) but for the AGCM experiment.

Geophysical Research Letters

Supporting Information for

Modulation of North American Heat Waves by the Tropical Atlantic Warm Pool

Hosmay Lopez[1], Dongmin Kim[2], Robert West[3], and Ben Kirtman[2].

[1]Atlantic Oceanographic and Meteorological Laboratory, NOAA, Miami, Florida, USA

[2]Cooperative Institute for Marine and Atmospheric Studies, University of Miami, Miami, Florida, USA

[3]Northern Gulf Institute, Mississippi State University, Mississippi State, MS, USA

Corresponding author address: Hosmay Lopez (NOAA/AOML/PHOD) 4301 Rickenbacker Causeway, Miami, FL 33149, USA. E-mail: Hosmay.Lopez@noaa.gov

Contents of this file

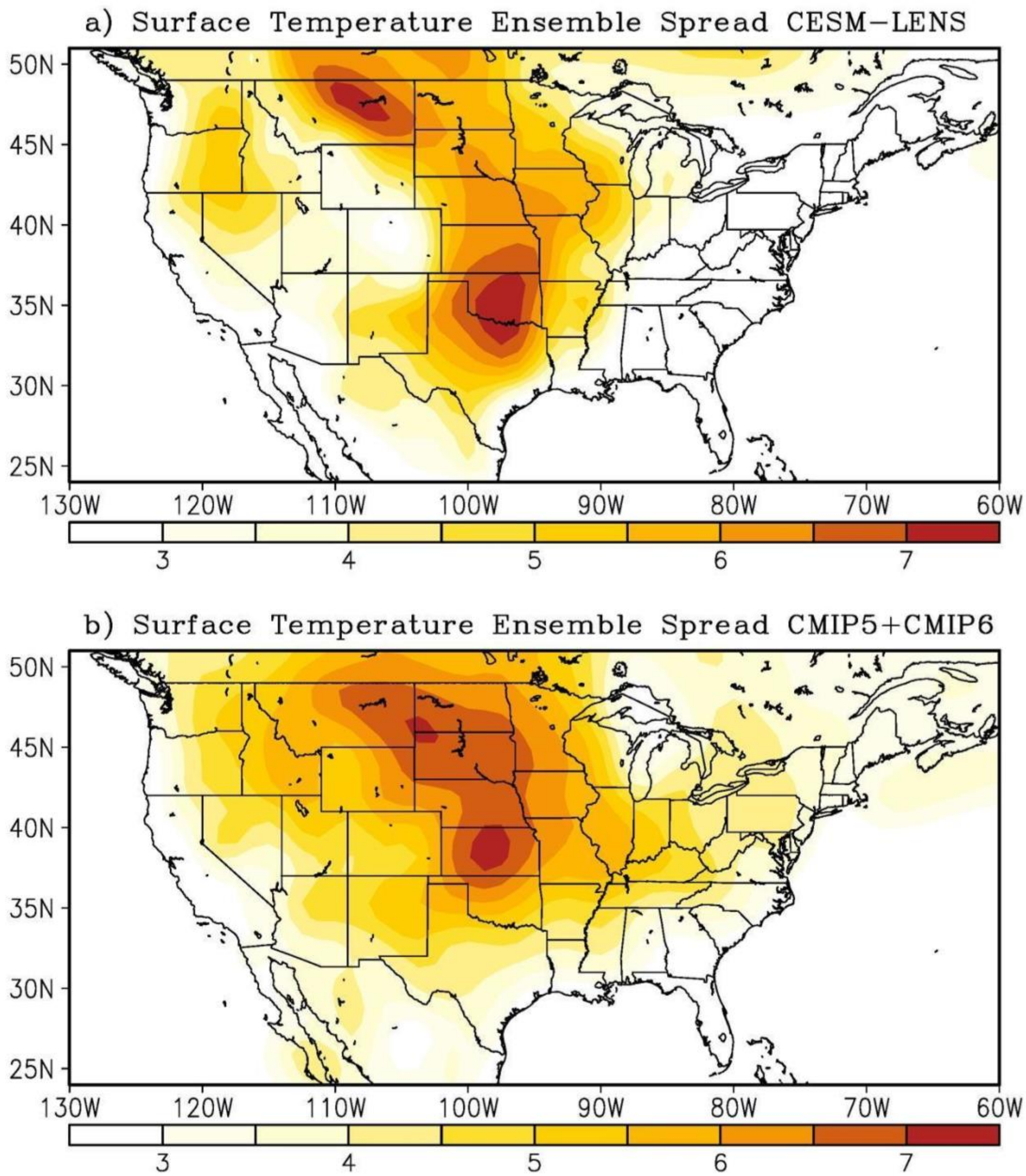

Supplementary Figure 1. Surface air temperature multi-model ensemble spread [◦C] for a) the CESM-Large Ensemble and b) several CMIP5 and CMIP6 models. For CESM-LENS, the ensemble spread is a measure of natural variability. For CMIP5 and CMIP6, the ensemble spread measures natural variability and differences in model physics.

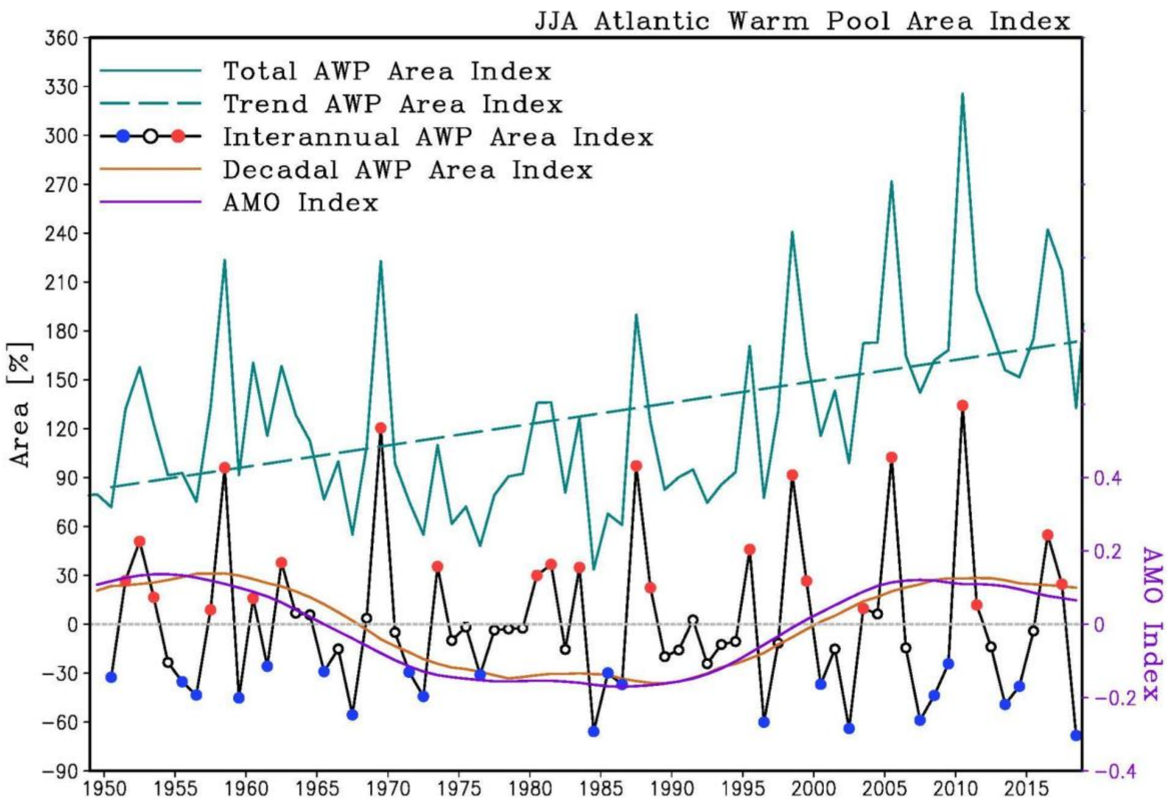

Supplementary Figure 2. June-July-August (JJA) Atlantic Warm Pool (AWP) area index and its decomposition into the linear trend, decadal and multidecadal, and interannual components. The normalized AMO index is also included for reference (purple). For the interannual AWP component, the years of large (red circle), near normal (open circle) and small (blue circle) AWP are highlighted. The AWP indices are shown as % change from the climatological AWP size.

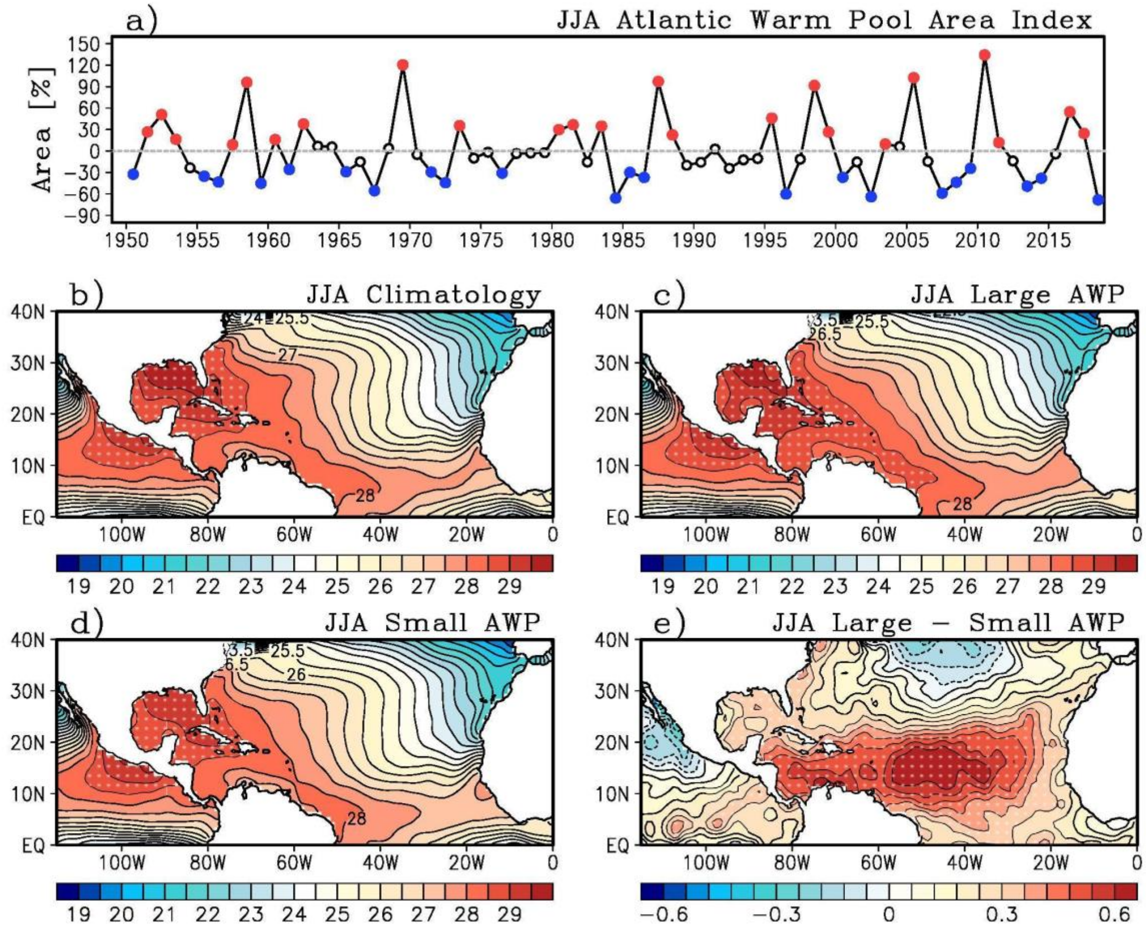

Supplementary Figure 3. a) June-July-August (JJA) Atlantic Warm Pool (AWP) area index. The years of large (red circle), near normal (open circle) and small (blue circle) are highlighted. (b-d) Composite SST during large, neutral, and small AWP area index. (e) Composite difference between large and small AWP. Large and small AWP are defined as the upper and lower terciles of the AWP area index. Contours greater than 28.5°C are stippled white. SST data from Hadley Centre.

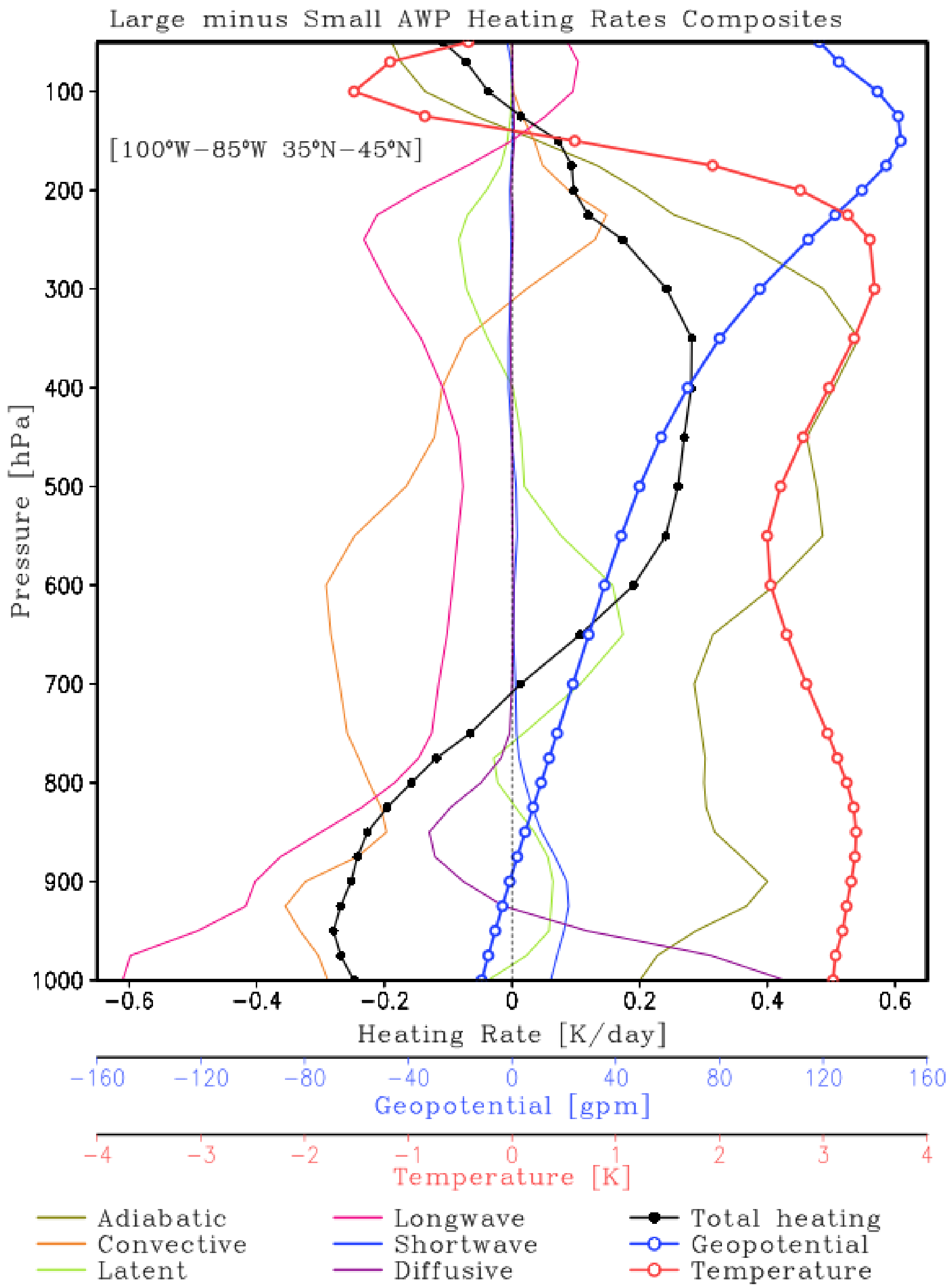

Supplementary Figure 4. Composite difference of large minus small AWP years during JJA for vertical profiles of different heating rates, geopotential height, and temperature anomalies. All variables are area-averaged over 100°W-85°W and 35°N-45°N, which comprises the US Great Plains region. All heating rates are obtained from JRA55.

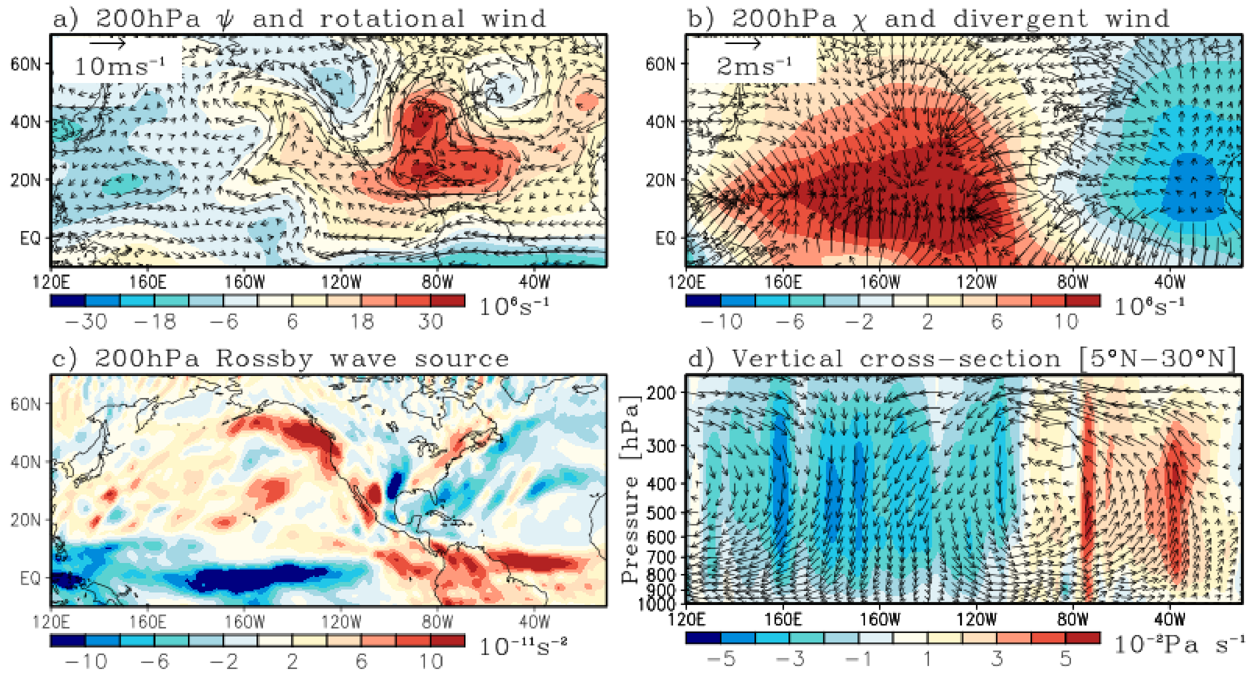

Supplementary Figure 5. Composite difference of large minus small AWP years during JJA for a) 200 hPa streamfunction (color, $10^6\ s^{-1}$) and 200 hPa rotational wind (vector, $m\ s^{-1}$), b), 200 hPa velocity potential (color, $10^6\ s^{-1}$) and 200 hPa divergent wind (vector, $m\ s^{-1}$). c) 200 hPa Rossby wave source where positive (negative) values indicate cyclonic (anticyclonic) source. d) cross section of vertical velocity (color, $10^{-2}\ Pa\ s^{-1}$) and zonal and vertical wind (vector) averaged from 5°N-25°N.

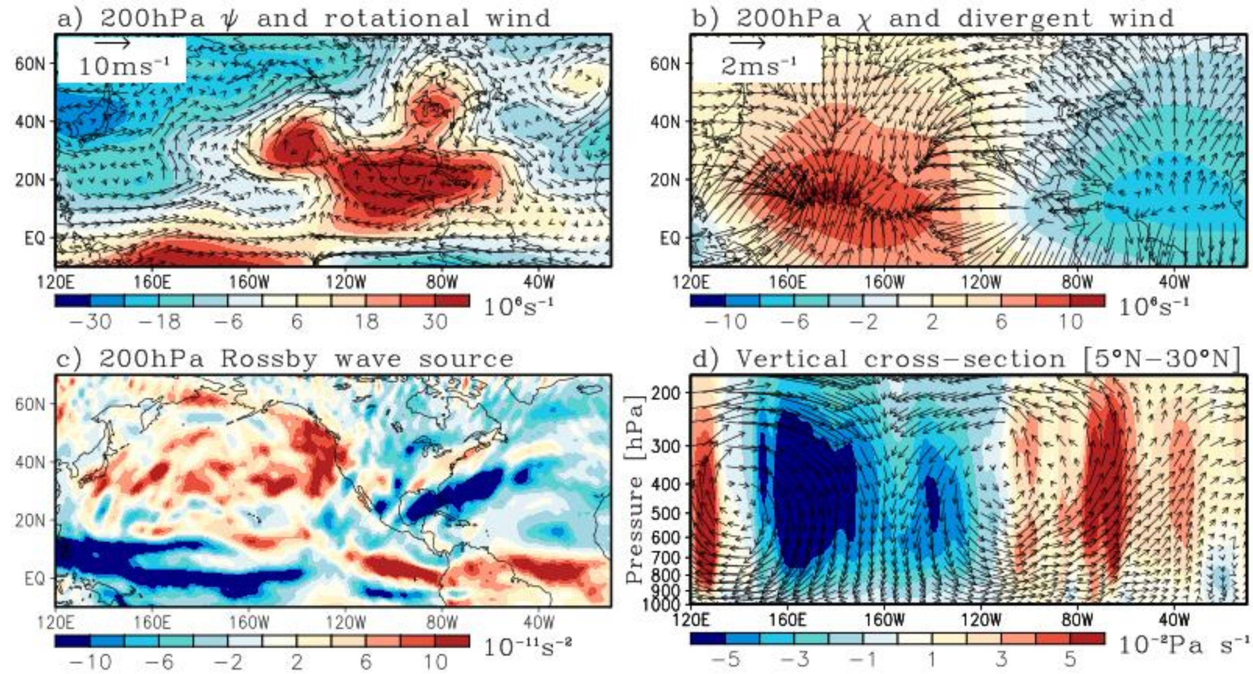

Supplementary Figure 6. Regression of the second principal component of JJA 200 hPa streamfunction anomaly onto a) 200 hPa streamfunction (color, 10^6 s^{-1}) and 200 hPa rotational wind (vector, m s^{-1}), b), 200 hPa velocity potential (color, 10^6 s^{-1}) and 200 hPa divergent wind (vector, m s^{-1}). c) 200 hPa Rossby wave source where positive (negative) values indicate cyclonic (anticyclonic) source. d) cross section of vertical velocity (color, 10^{-2} Pa s^{-1}) and zonal and vertical wind (vector) averaged from 5°N-25°N. This second model explains 10% of the total variance of JJA 200 hPa streamfunction anomalies.

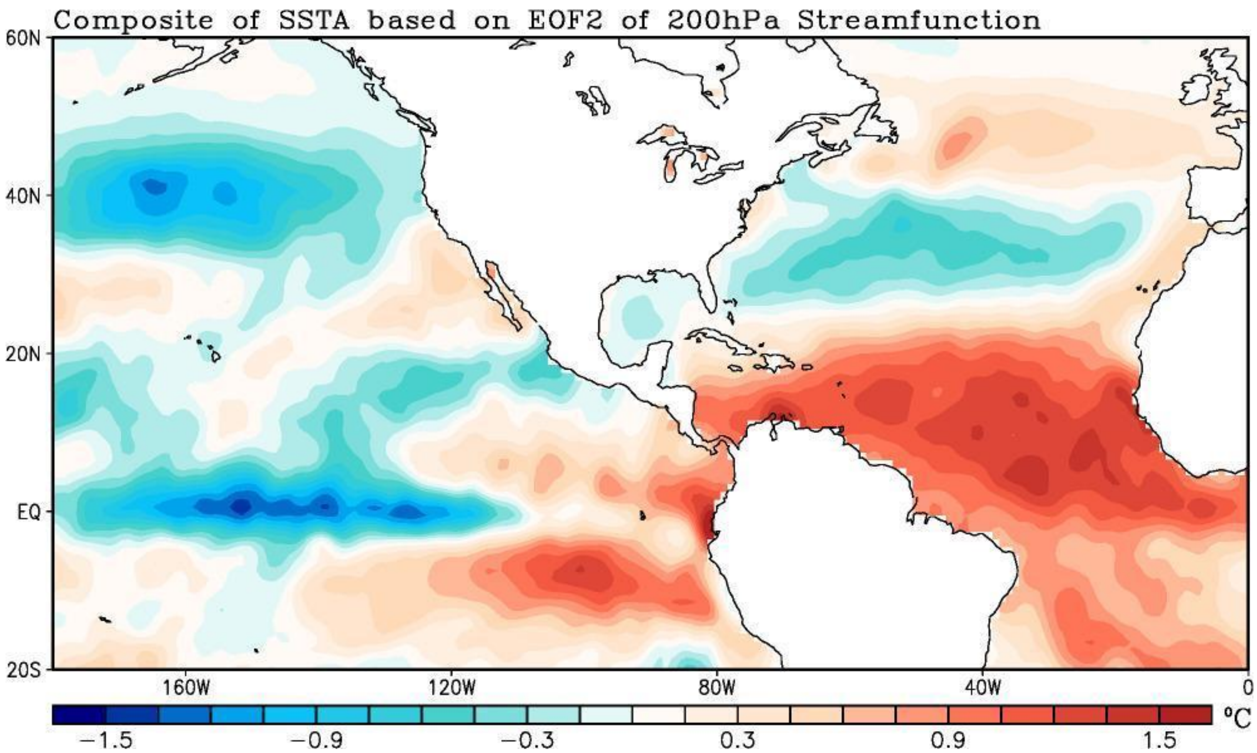

Supplementary Figure 7. Same as Supplementary Fig. 6 but for the regression of the second principal component of JJA 200 hPa streamfunction anomaly onto observed SST anomalies.

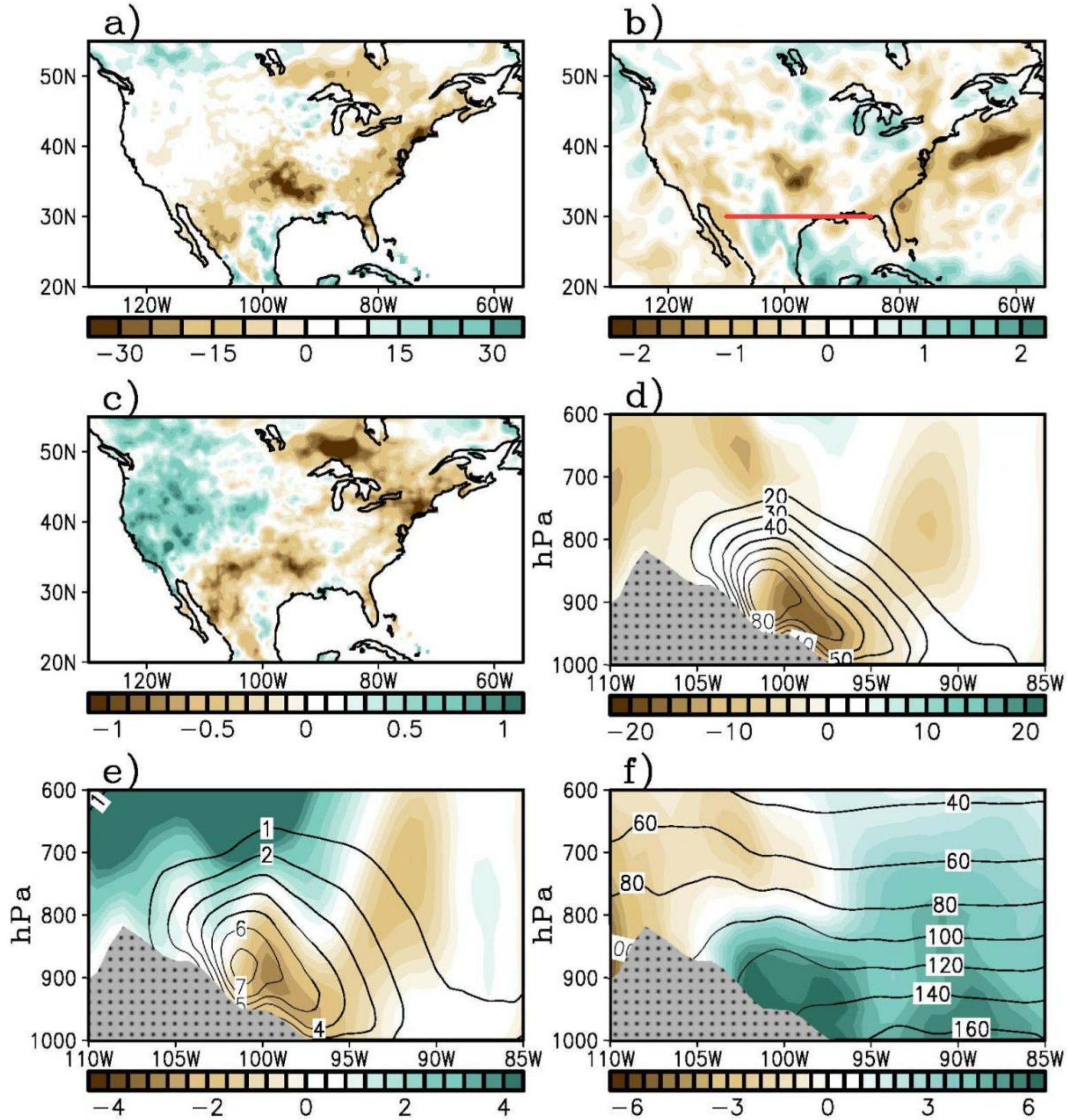

Supplementary Figure 8. Composite difference of large minus small AWP years during JJA for a) precipitation (*mm day*$^{-1}$), b) vertically-integrated moisture transport divergence (*Kg m*$^{-2}$ *s*$^{-1}$) with negative values indicating divergence, c) standard precipitation index. d) cross section of meridional moisture transport composite difference of large minus small AWP (color) and its JJA climatology (black contour) at 30°N from 110°W-85°W, which is highlighted by red line in panel b). e) same as d) but only accounting for changes in meridional wind during large minus small AWP. f) Same as d) but only accounting for changes in moisture during large minus small AWP.

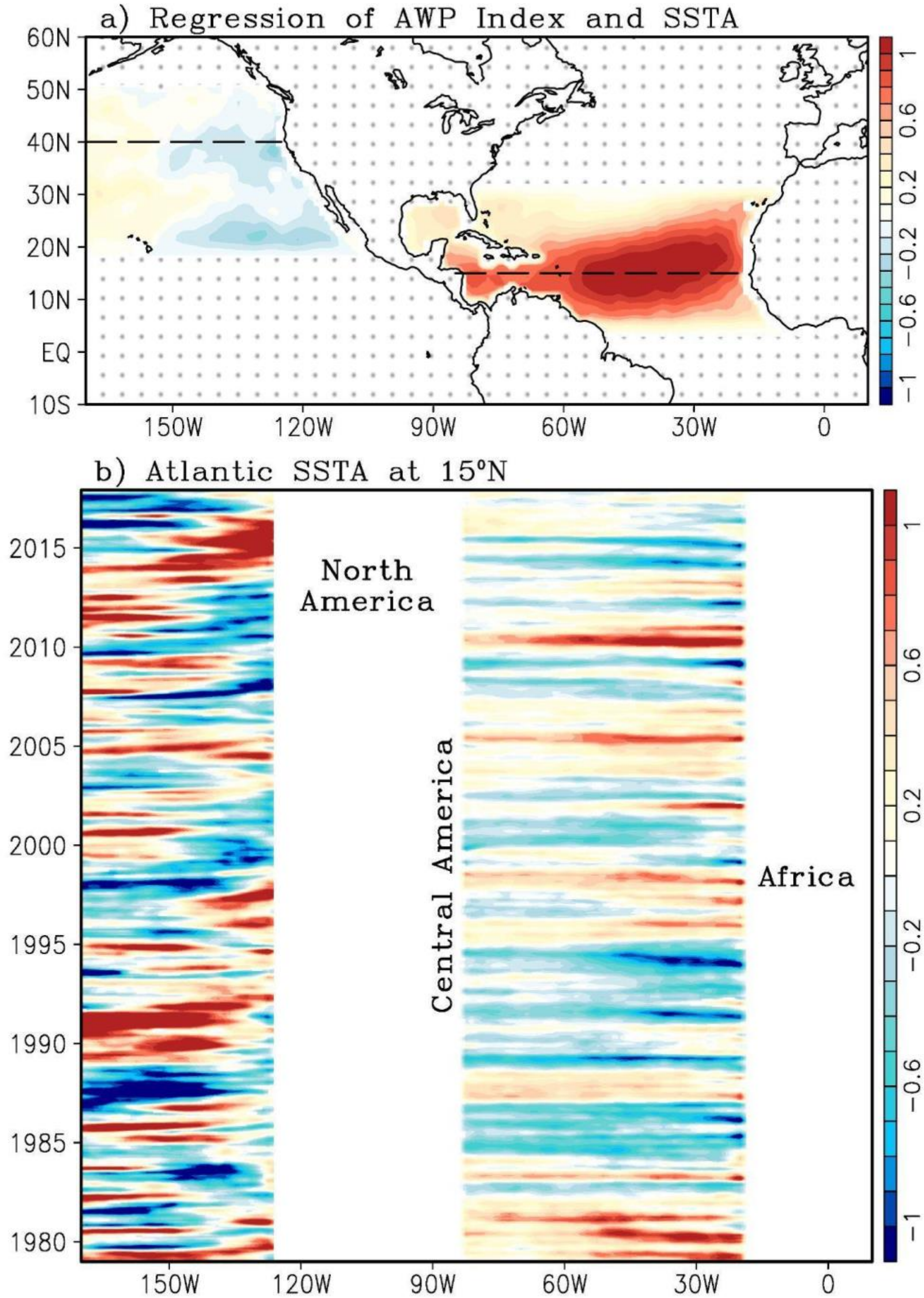

Supplementary Figure 9. a) Regression of June-July-August (JJA) sea surface temperature anomalies (SSTA, °C) and AWP area index masked over the tropical Atlantic and extra-tropical Pacific regions used to force the AGCM experiments. b) Observed (1979-2017) SSTA at 15°N for the Atlantic and 40°N for the Pacific basins used to force the AGCM experiments. Note that in all other regions, SSTs are held to their climatology.

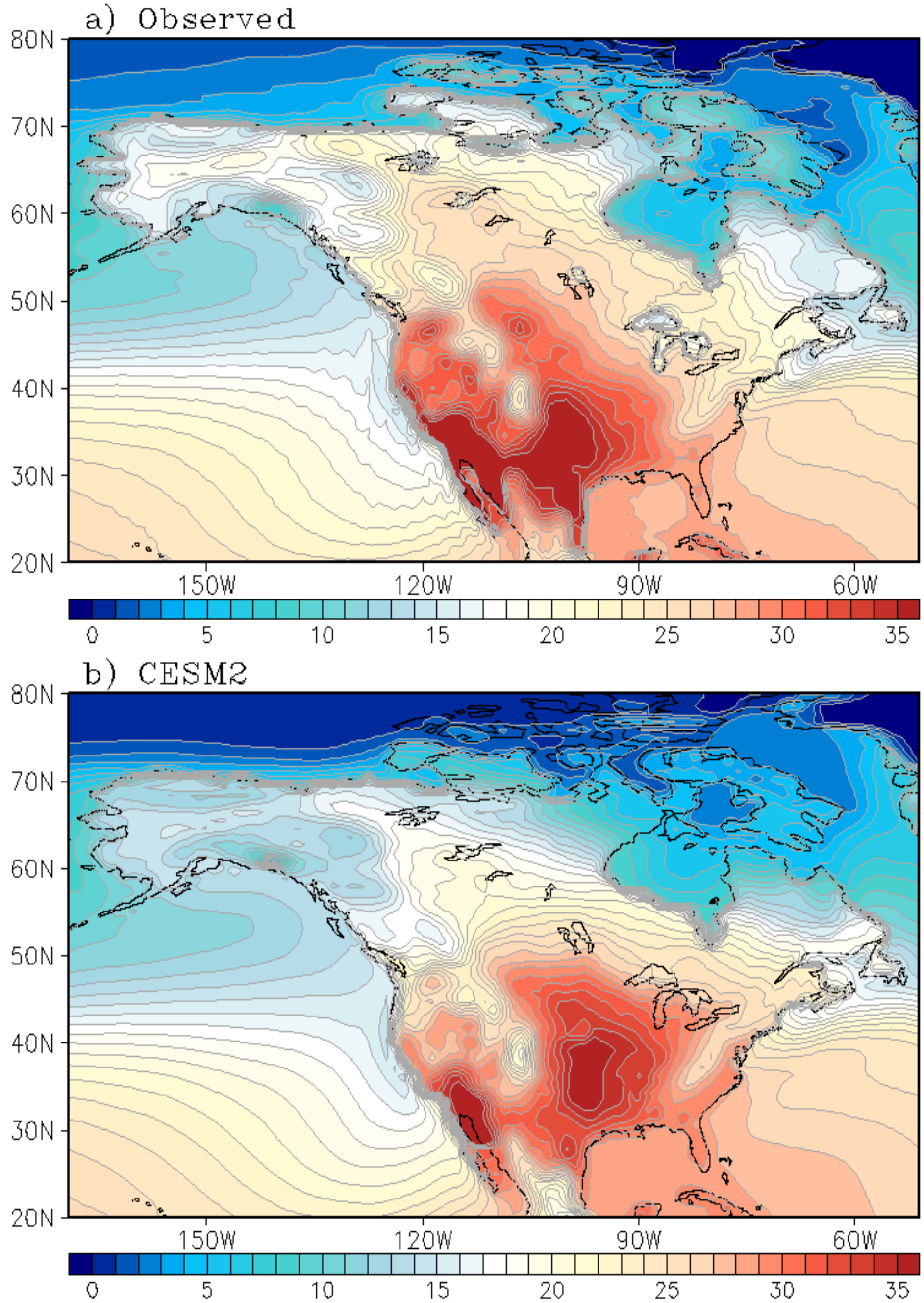

Supplementary Figure 10. Ninety-fifth percentile (T_{95}) threshold of daily mean surface temperature for a) observed and b) CAM6 model used here to perform AGCM experiments.

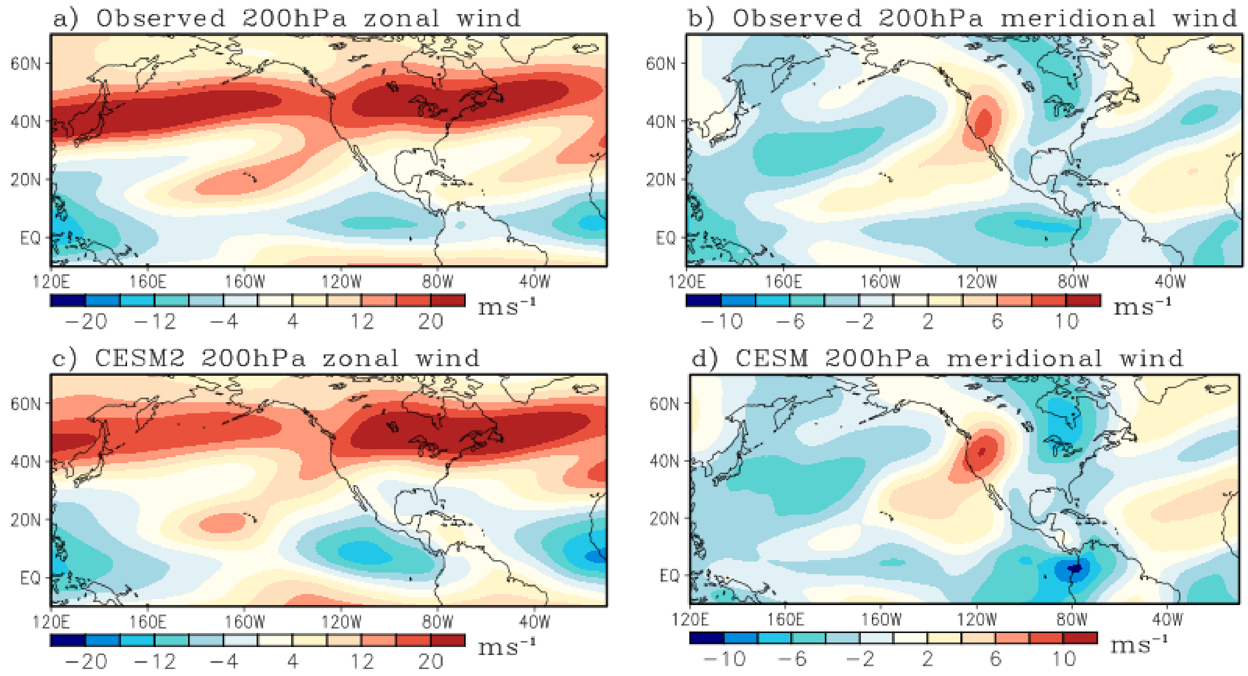

Supplementary Figure 11. Observed JJA mean a) 200 hPa zonal and b) 200 hPa meridional wind. c) and d) are similar to a) and b) but for the AGCM model simulation respectively.

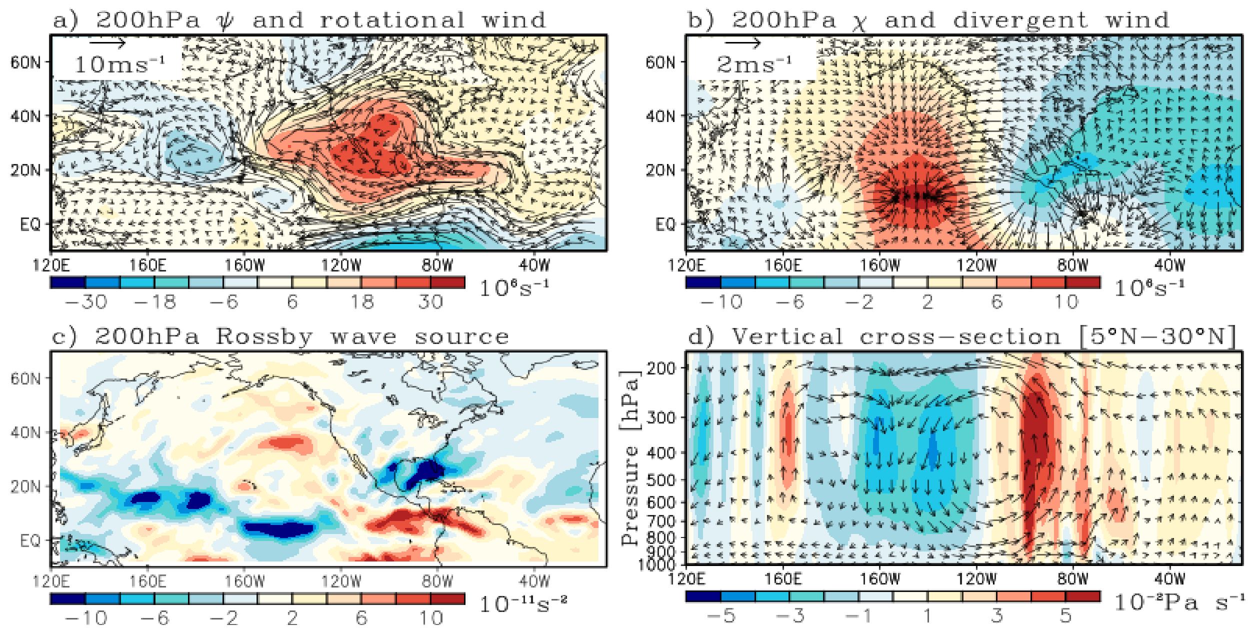

Supplementary Figure 12. Same as Supplementary Fig. 5 but for the AGCM model simulation. All plots are composite differences of large minus small AWP years.

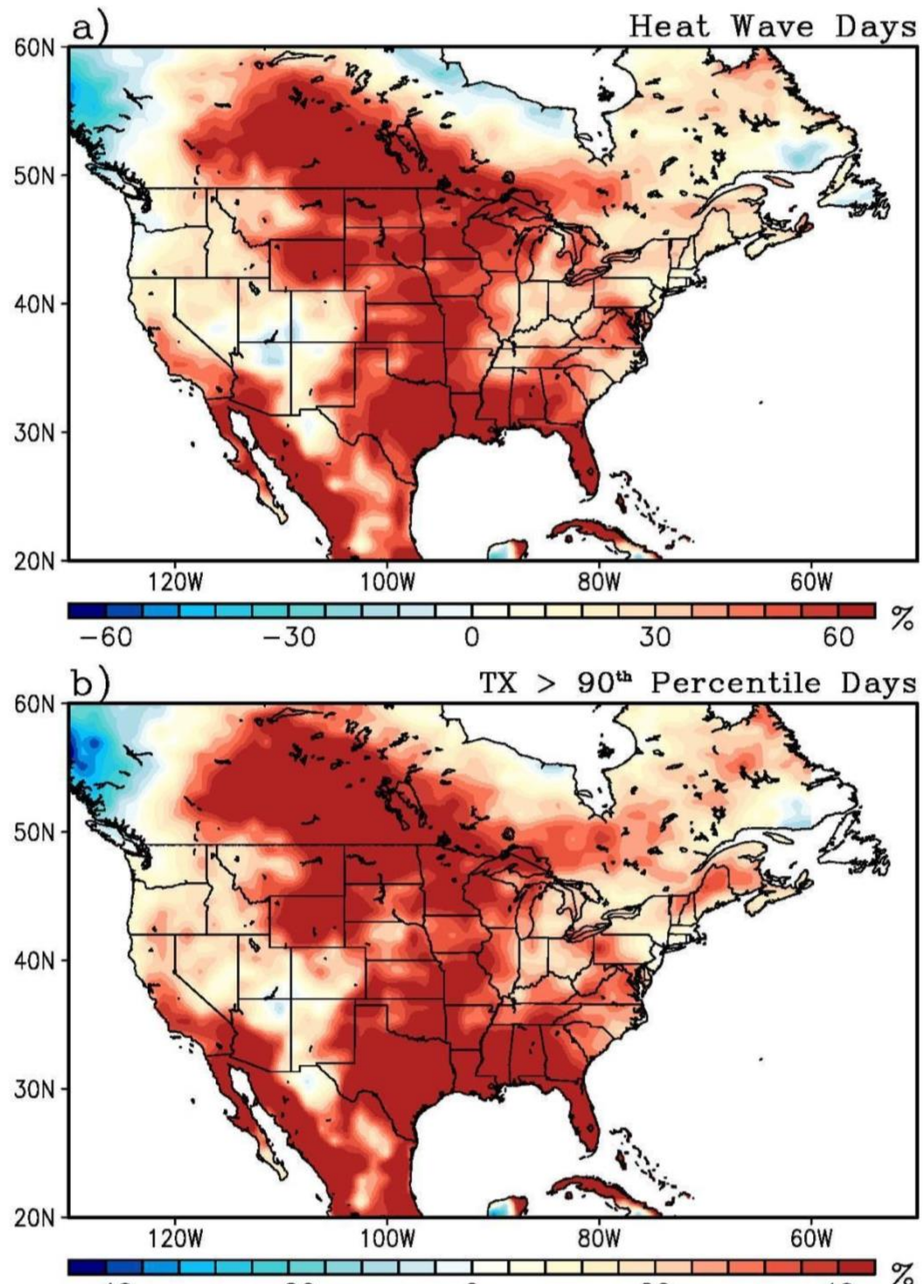

Supplementary Figure 13. Composite difference of large minus small Atlantic Warm Pool years during JJA for a) number of heat wave days and b) number of days with maximum temperature exceeding the 90th percentile from the 200-year AGCM model simulation.